



OPEN

Characterization of complex fluvial-deltaic deposits in Northeast India using Poisson impedance inversion and non-parametric statistical technique

M. Nagendra Babu✉, Venkatesh Ambati & Rajesh R. Nair

Characterizing complex fluvial-deltaic deposits is a challenging task for finding hydrocarbon discoveries. We described a methodology for predicting the hydrocarbon zones from complex well-log and prestack seismic data. In this current study, data analysis involves an integrated framework based on Simultaneous prestack seismic inversion (SPSI), target correlation coefficient analysis (TCCA), Poisson impedance inversion, and non-parametric statistical analysis, and Bayesian classification. First, seismic elastic attributes from prestack seismic data were estimated. They can provide the spatial distribution of petrophysical properties of seismic data. Then target correlation coefficient analysis (TCCA) was estimated rotation factor “c” from well-log data. Using the seismic elastic attributes and rotation factor “c”, Poisson impedance inversion was performed to predict the Poisson impedance volume. Finally, Bayesian classification integrated the Poisson impedance volume with non-parametric probabilistic density functions (PDFs) to estimate the spatial distribution of lithofacies. Despite complex characteristics in the elastic properties, the current study successfully delineated the complex fluvial-deltaic deposits. These results were verified with conventional findings through numerical analysis.

The lithological types and the hydrocarbon saturation zone are essential in the characterization of reservoir¹. Modeling and characterization of lithology are critical in basin analysis and subsequent studies such as drilling and reservoir development studies². The most difficult challenge in reservoir studies is obtaining accurate lithology and fluid saturation zones from various sources, particularly seismic data³. The most uncertainty is related to seismic information due to low resolution, non-unique solutions of seismic inversion techniques, and the relation between well-log and seismic data^{4,5}.

The geoscientist's quest in the seismic interpretation defines the relationship between geophysical Data (Seismic data and well data) and reservoir properties to predict lithology distribution and mapping fluid-saturated zones⁶. Geoscientist's frequently used seismic elastic characteristics and rock physical constants to distinguish lithologies and locate hydrocarbon-saturated zones⁷. Seismic elastic attributes such as P-impedance (Z_p), S-impedance (Z_s), density (ρ), and V_p/V_s ratio are used for lithology characterization by incorporating wireline log data⁸. Rock physical attributes such as Young modulus (E), shear modulus(μ), bulk modulus(k), Lambda-rho (λ), and Mu-rho ($\mu\rho$) have been used to identify hydrocarbon saturated zone⁹. Several methods have been proposed in quantitative seismic interpretation to estimate fluid-saturated zones and identify different rock types^{10,11}. For a few years, seismic elastic properties have been used to discriminate hydrocarbon zone from other zones (Brine sand and shale)^{12,13}. The seismic inversion technique (prestack inversion and AVO analysis) has become essential for understanding elastic properties (Z_p , Z_s , ρ & V_p/V_s ratio) of lithology types and petrophysical parameters¹⁴. A study explained the practical approach by the different seismic inversion techniques to identify the lithofacies¹⁵. Another study explained lithofacies classification from seismic inversion in a geothermal reservoir¹⁶. Another researcher differentiated rock type based on petrophysical properties and estimated the permeability zones¹⁷.

Computational Petroleum Geomechanics Laboratory, Department of Ocean Engineering, Indian Institute of Technology Madras, Chennai, India. ✉email: oe16d022@smail.iitm.ac.in

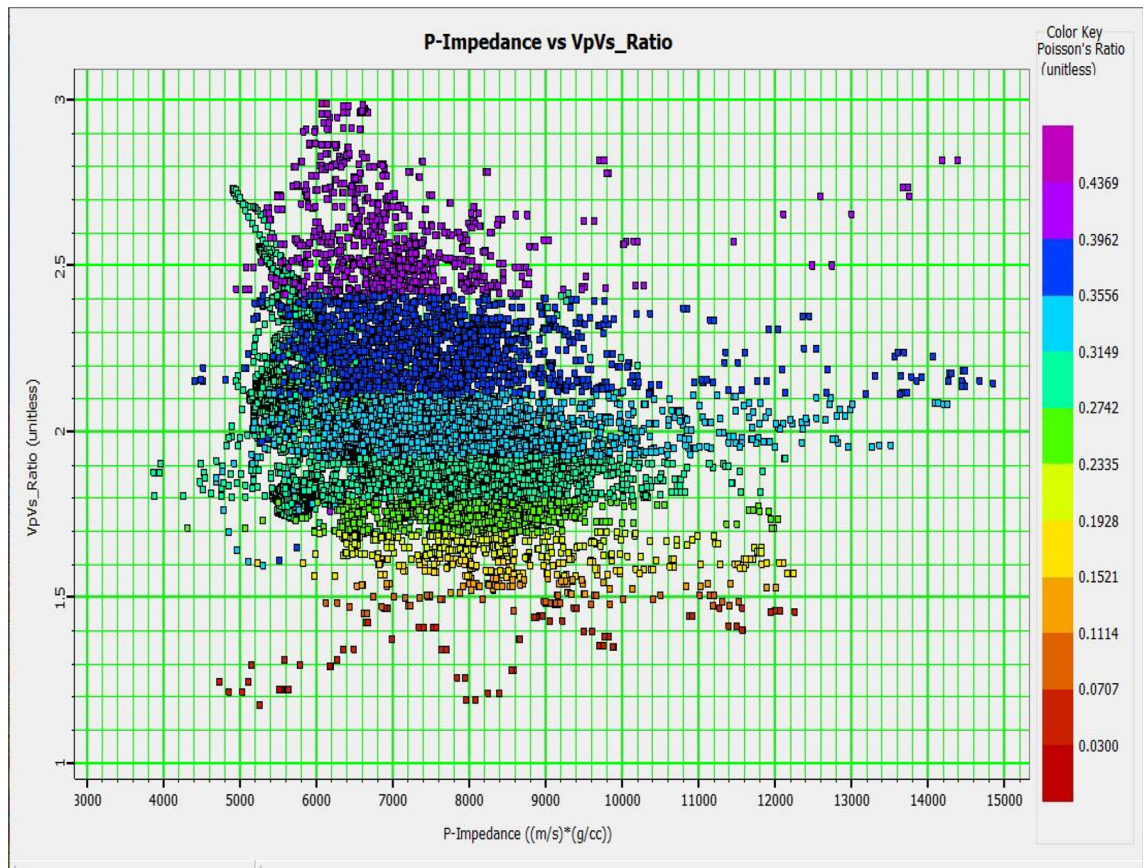


Figure 1. Cross plot of acoustic impedance (Z_p) and V_p/V_s ratio.

Characterizing the prospective zones from the other lithological zones in some reservoirs is very challenging if all have similar characteristics¹⁸. A study characterized the low resistivity low contrast reservoirs using the lithology impedance attribute¹⁹. Conventionally, low Poisson ratio and low-density values indicate hydrocarbon in many reservoirs, and those values are separated in a cross-plot if the lithology is clean sand²⁰. However, the sand quality might be different and not as clean in reality. Many difficulties are encountered when those elastic properties have similar properties, and characterizing lithologies can be complex²¹. Figure 1 shows the Z_p and V_p/V_s ratio cross plot in the study area. Here observed, no proper separation of data points in the cross plot. As the color code of data points mentioned, the low Poisson ratio values belong to the hydrocarbon zone, but Z_p range values are almost the same for all zones. So only the Poisson ratio or V_p/V_s ratio plays a significant role in the classification.

On the other hand, rock physical analysis can be applied to create the relation between rock properties (well log data) and seismic attributes²². Rock physics template (RPT) based on cross-plot analysis uses different rock properties to identify hydrocarbon saturated zone and lithology²³. However, since an oil reservoir has indistinguishable elastic properties from lithologies and fluid-saturated zones, conventional techniques such as prestack inversion, AVO analysis, and RPT are not enough to explicitly characterize brine hydrocarbon zones²⁴.

A notable attribute named Poisson impedance (PI) was introduced to address the issues faced in those reservoirs²⁵. The PI has defined as the difference between Z_p and scaled Z_s . Poisson impedance helps characterize a reservoir with fluid content as an elastic constant. Poisson impedance inversion has given remarkable accomplishments in distinguishing different lithologies in the oil and gas industry²⁶. The PI is used as a fluid factor in identifying the fluid content in the sandstone reservoir²⁷. A scaled factor in the Poisson relation is crucial for Poisson impedance inversion success. A scale factor (c) is measured from the slope of the cross plot between compressional impedance (Z_p) and shear impedance (Z_s). An accurate measure of " c " is a critical task for the meaningful interpretation of PI¹⁸.

The Target correlation coefficient analysis (TCCA) was used in this study to estimate the accurate rotation parameter " c "²⁸. The TCCA method has been used in many studies to estimate the " c " factor²⁹. The hydrocarbon reservoir was characterized by Poisson impedance inversion, which used the TCCA to estimate factor " c "³⁰. The TCCA can be applied to the GR, resistivity, and water saturation log. GR log can be used for lithofacies classification, and the resistivity log can be used for fluid classification through the fluid impedance³¹.

The non-parametric statistical classification based on the kernel density estimator was implied in this study to estimate the Probabilistic Density Functions (PDFs)³². The kernel density estimator of non-parametric statistical classification was suitable for geophysical data like well-log data³³. A study has discussed lithology prediction using the borehole data using the non-parametric density estimator³⁴. In many studies, kernel density estimators

are efficiently distributed classes comparable to parametric methods³⁵. The bandwidth (h) of the kernel operator is the single parameter to be determined in non-parametric kernel estimation. The kernel-based non-parametric statistical method provides smoother density functions³⁶. Unlike the parametric method, these classification methods do not require predefined parameter assumptions/restrictions. As in the parametric method, assumptions of PDFs are complicated for geophysical data. So this non-parametric kernel estimator avoids the significant restrictions of the parametric approach³⁷. Finally, the Bayesian approach was used in this study to estimate lithology volume for lithologies by combining the PDFs of non-parametric kernel estimator and seismic inputs (Poisson impedance & V_p/V_s ratio). The Bayesian classification methodology is convenient for dealing with complex problems³⁸. The Bayes' rule can integrate the different data sources and analyze the uncertainty³⁹.

This study adopted a workflow to predict the hydrocarbon saturated zone of a sandstone reservoir of the Tipam formation from the Upper Assam basin, India. The study area has similar seismic velocities and density values for different lithologies such as shale, brine sand, and hydrocarbon sand. These issues make it challenging to characterize the accurate fluid and lithology, which was impossible in conventional interpretation techniques.

Geological setting. The Assam-Arakan Basin is a petroleum-rich province in Northeast India, consisting of various tectonic-controlled basins⁴⁰. The eastern Himalayas bounded the Basin in the North, Mikir hills in the southwest, and Naga hills at the southeastern boundary⁴¹. The Upper Assam basin contains the depositional system from the Eocene to Mio-Pleistocene. The essential litho-units are the Tipam sediments and Girujan clay of the Miocene age, Barail formation from the Oligocene age, and Sylhet Limestone and Kopili formation from the Eocene⁴². However, every stratigraphic horizon from Miocene has shown indications of hydrocarbon deposits. The crucial source rocks are the coal-shale unit of the Barial group from the Oligocene age, the shale of Koplili formation from Eocene, and Sylhet/Tura's formations of Paleocene. Girujan clays in the Assam Shelf on the northern side and Bokabil clays on the southern part act as major seals in the Upper Assam Basin⁴⁴. Furthermore, many interbedded shale bands within the Oligocene formation also act as the local seals within the group.

The target reservoir is the Tipam formation contains the significant producible sediments belonging to the Miocene age, deposited in the fresh-brackish water ecosystems in the Assam Basin⁴³. This formation has been subdivided into Upper, Middle, and Lower Tipam. The middle Tipam formation has the sand/shale alteration sequence, and the Lower Tipam formation consists of the Arenaceous sequence⁴⁴. The upper Tipam contains an arenaceous sequence. Oil and gas occur in Tipam sands with porosity ranging from 15 to 22%.

The data for analysis were borehole logs and prestack 3D seismic data volumes. The borehole logs have compressional slowness (DTCO), shear transit slowness (DTSM), density (ρ), resistivity logs (LLS, LLD & MSFL), and Gamma-ray (GR), Neutron porosity (NHPI) logs. After pre-conditioning, the seismic offset gathers have converted into angle gathers, which are required for prestack inversion. Well#A and Well#C was used for inversion and cross-plot analysis. Other well-logs are kept for quality check of inversion and classification results. Figure 2a shows available well-logging curves of Well#03, and Fig. 2b shows raw seismic offset gathers of the study area.

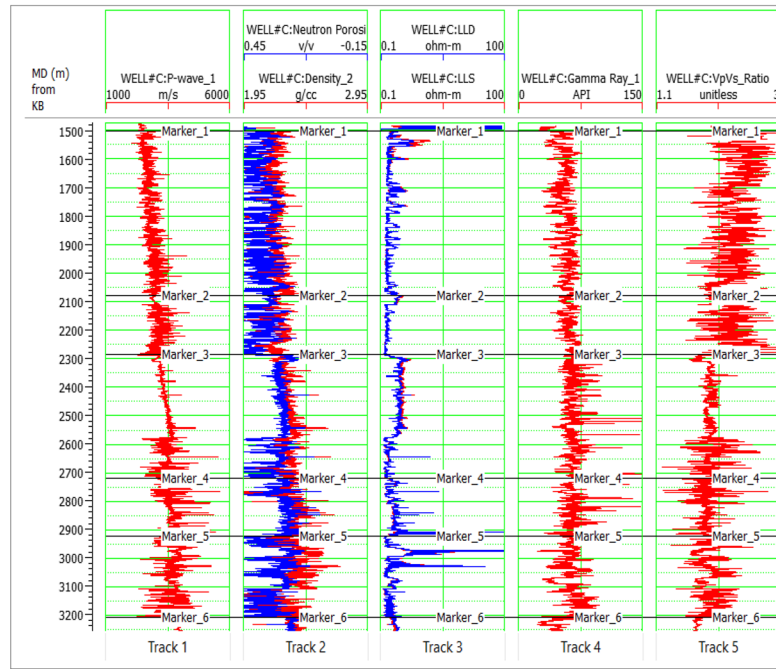
Results and discussion

Seismic attributes determination. The SPSI technique was performed using the prestack seismic data and well-logs (Well#A & Well#C). We took advantage of SPSI in the generation of shear properties along with acoustic properties. This method transforms the prestack seismic data (angle gathers) into meaningful petrophysical parameters Z_p , Z_s , V_p/V_s ratio, and density. The prestack inversion involves wavelet extraction (statistical and well based), well to seismic tie, estimation of the background model, and deterministic optimization using the simultaneous prestack inversion technique. Prestack angle gathers are inverted into elastic properties using well-based angle-dependent wavelets and an initial low-frequency model. Figure 3 shows an arbitrary line of inverted seismic volumes (Z_p & Z_s) intersecting all wells, and inverted results were verified with inserted well properties (Z_p & Z_s) in the seismic data.

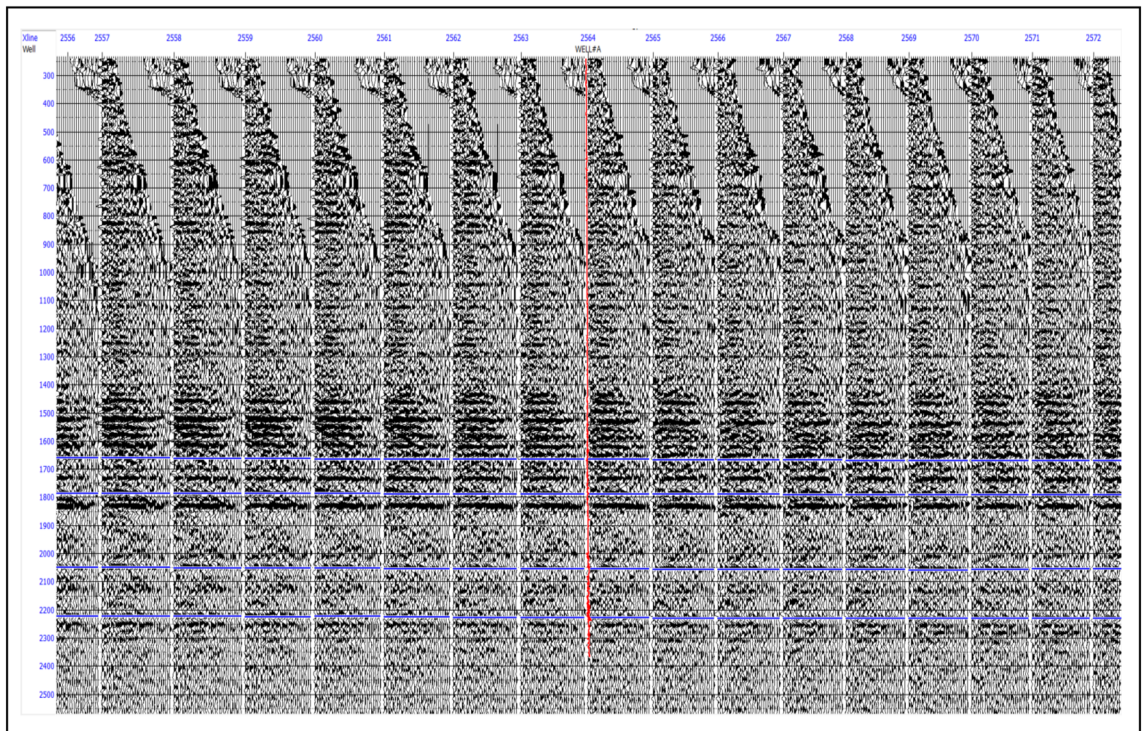
As mentioned earlier, conventional interpretation attributes such as Z_p & V_p/V_s ratio are used to classify the lithofacies. As seen in Table 1, conventional attribute Z_p is almost similar for classified lithofacies. As mentioned earlier, only V_p/V_s ratio influences lithofacies characterization. This depositional complexity is difficult to classify with conventional attributes.

Poisson impedance (PI) volume extraction. PI analysis was conducted as the second step of the methodology to estimate PI attribute volume from seismic elastic attributes and PI curves from well log data. An accurate value of rotation factor "c" is required to estimate the Poisson impedance volume, as mentioned in Eq. (2) in the material and methodology section. This rotation factor is generally obtained from regression analysis on the cross-plot of Z_p and Z_s . However, TCCA was utilized to predict the accurate value of the rotation factor "c". The correlation analysis was conducted using the GR log and the PI curves obtained by different "c" values. This correlation analysis shows a maximum correlation coefficient at the c-value of 1.4553 for the GR curve ($cc = 0.685$). This "c" value can be used to estimate Poisson impedance volume. Figure 4 shows the target correlation coefficient analysis to estimate the "c" value.

As mentioned²⁵ in Eq. (2), Poisson impedance inversion was performed using the estimated rotation factor "c" and seismic elastic volumes such as AI and SI. The PI inversion was applied to seismic volumes and borehole logs. The PI volume and curves were created using the Z_p , Z_s , and "c" factor (1.4553). The Arbitrary PI volume from seismic attributes is shown in Fig. 5. Figure 5 shows PI attributes volume that reveals that the hydrocarbon zone was observed to have a well-defined separation with the effectiveness of the PI attribute. Low PI values ranging from 500 ((m/s) * (g/cc)) to 1450 ((m/s) * (g/cc)) indicates the hydrocarbon zone as classified in cross plot analysis (Fig. 6a). PI values 1450–2100 ((m/s) * (g/cc)) indicates water-bearing sand lithology. PI values ranging from 2100–3200 ((m/s) * (g/cc)) corresponding to shale.



a:



b:

Figure 2. (a) Well logging curves of Well#03 in the study area. (b) Seismic Raw data (offset gathers) used in this study.

Lithological characterization by non-parametric statistical technique and Bayesian classification. This section determines the spatial distribution of lithofacies by applying Bayesian classification using the non-parametric PDFs and Poisson impedance attribute. Mathematical information is provided in the methodology section. First, cross-plot analyses are generally conducted to separate different lithologies using seismic and well-log data⁴⁵. The relation of different attributes is visually represented by cross plots for interpreting the hydrocarbon's presence and other lithologies. Different attribute pairs can be used to identify the lithologies by

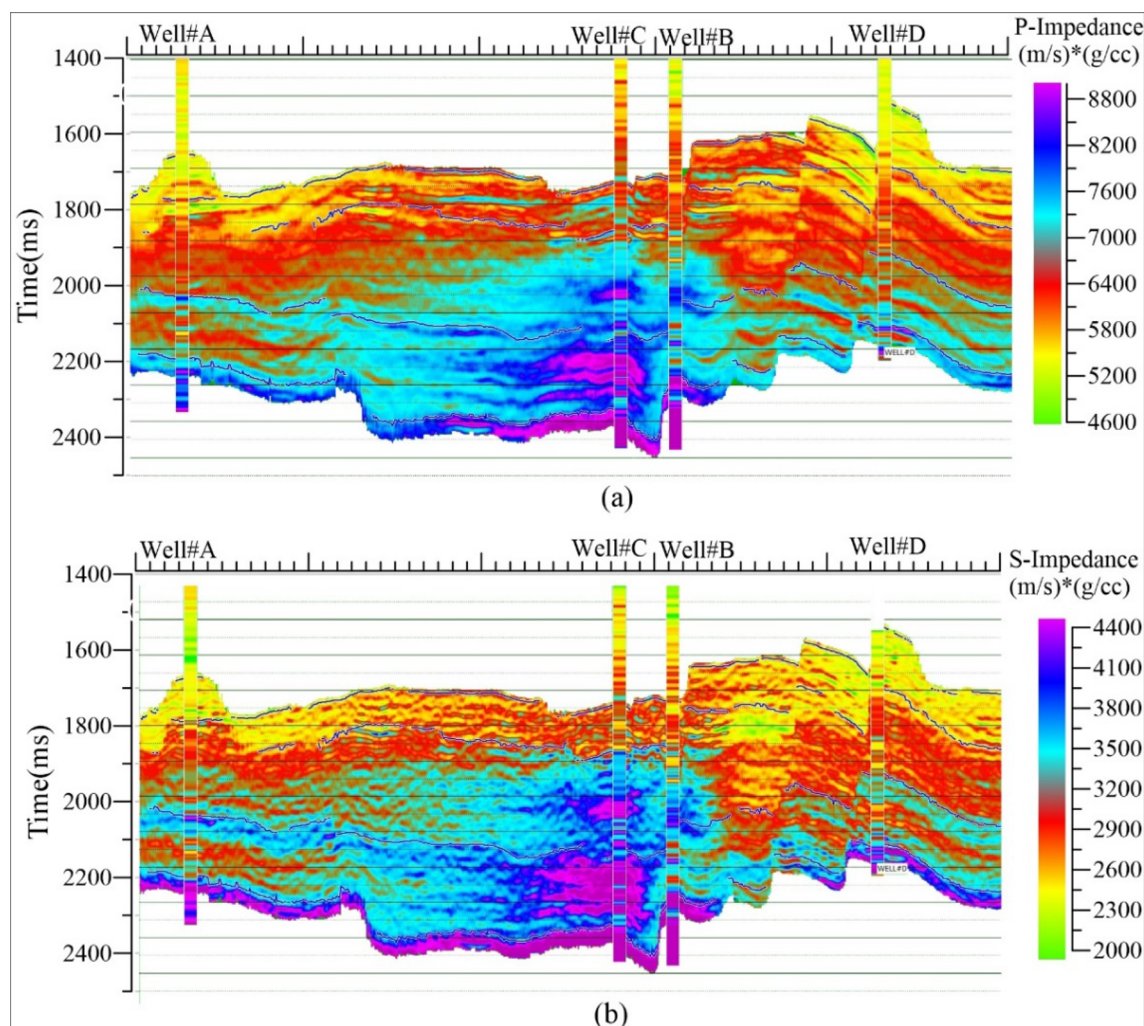


Figure 3. An arbitrary line of SPSI results along with well locations: (a) acoustic impedance, (b) shear impedance.

Lithofacies class	P-Impedance (Z_p) ((m/s) (g/cc))	V_p/V_s ratio
HC	3800–12,400	1.15–1.82
SAND	3500–14,900	1.82–2.12
SHALE	3500–13,900	2.12–3.1

Table 1. Interpreted ranges of conventional attributes for lithofacies classification.

making clusters on data points of cross-plot⁴⁶. The cross-plot analysis was performed using the PI curves and V_p/V_s ratio of Well#A and Well#C to characterize various lithofacies. Figure 6a shows cross-plot analysis, which was characterized as hydrocarbon-bearing zones with red color, sand with yellow, and shale with green. Table 2 shows PI & V_p/V_s ratio values to characterize the different lithologies.

The non-parametric statistical mechanism was performed on the cross-plot data points (Fig. 6a) to estimate PDFs for each lithofacies. As mentioned in the methodology section, there is no parameter estimation in non-parametric statistical techniques for predicting PDFs. Based on the non-parametric methodology, different bandwidth (h) tried to estimate the PDFs and lithofacies prediction results verified with confusion matrix at well locations (Well#A and Well#B). The confusion matrix was applied between true lithofacies (from Well logs) and predicted logs (seismic lithofacies at well locations). Seismic lithofacies are estimated by integrating the seismic attributes and PDFs using Bayes' rule¹. Here we finalized bandwidth as 4.93, which provided a better confusion matrix. The non-parametric PDFs for three lithofacies are shown in Fig. 6b.

The confusion matrix and visual comparison between the true and predicted lithofacies of Well #A and Well#C are shown in Fig. 6c,d. The column data in the confusion matrix was true data, and the row data represented predicted data. The more significant percentages in the confusion matrix indicate the quality of the

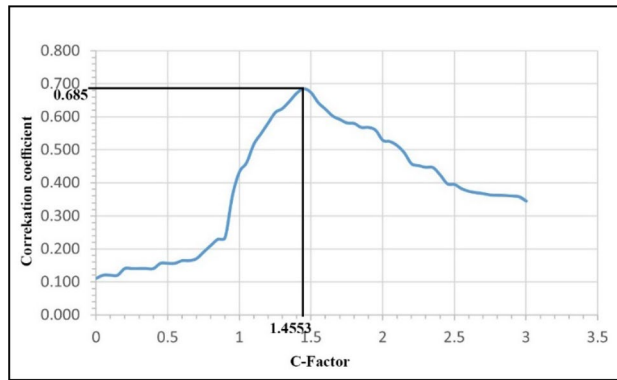


Figure 4. Rotation factor “c” estimation from the Target correlation coefficient analysis.

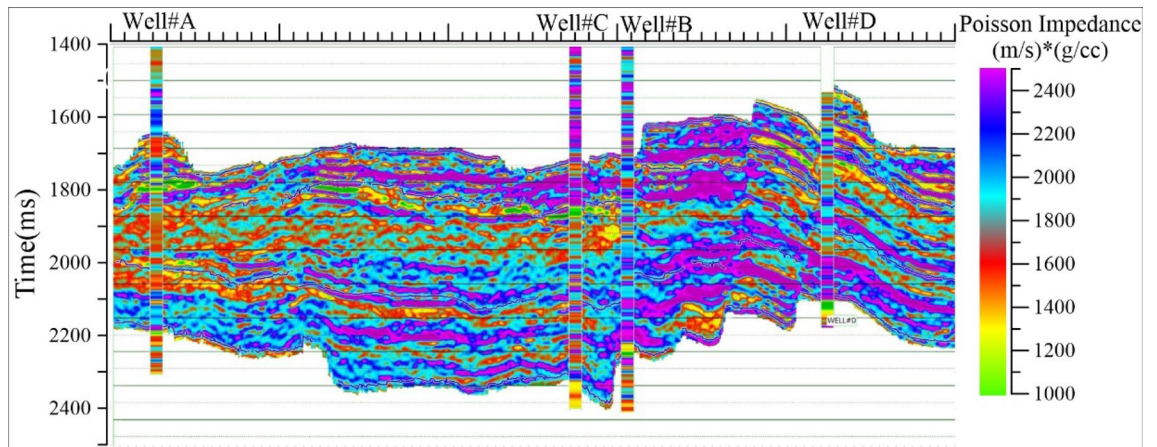


Figure 5. Arbitrary line of Poisson Impedance (PI) volume intersects at wellbore locations with PI property.

results if the high values indicate a good match between the true and predicted lithofacies. It provides mismatch information between true lithofacies and predicted lithofacies at well locations. Figure 6d visually inspects predicted lithofacies of Well#A and Well#C with corresponding true lithofacies. Using the non-parametric PDFs, litho-logs (estimated from cross-plot classification), and seismic input such as Poisson impedance & V_p/V_s ratio to estimate the lithofacies model by Bayesian classification. Lithologies help as prior information in Eq. 4⁴⁷. Figure 7 shows the arbitrary line of lithofacies volume with three lithofacies such as hydrocarbon zone (Red color), sand (yellow), and shale (Green), intersecting at all well locations.

In this study, the estimated Poisson impedance attribute helped to classify the lithofacies. As seen in Table 2, two attributes (PI and V_p/V_s ratio) play an important role in classifying lithofacies (Fig. 6a). Low PI (500–1450) ((m/s) * (g/cc) & low V_p/V_s ratio values (1.15–1.82) were identified as hydrocarbon saturated zone, marked as red color in the lithology model (Fig. 7). The brine sand was differentiated by PI values ranging from 1450 (m/s) * (g/cc) to 2100 (m/s) * (g/cc) & V_p/V_s ratio ranging from 1.60–2.45. The shale was modeled with values of PI 2100–3200 (m/s) * (g/cc) & V_p/V_s ratio 1.78–2.43. Figure 8a,b shows three-dimensional slices of conventional attributes (Z_p and V_p/V_s ratio) at 1820 ms in the seismic data. It was observed in Fig. 8a that acoustic values could not able characterize lithofacies due to almost similar values. However, PI impedance volume in Fig. 8c has clear separation values for different lithofacies, especially hydrocarbon zones. Figure 8d shows the horizontal slice of resultant lithofacies after applying Bayesian classification using the non-parametric PDFs, PI volume (Fig. 8c), and V_p/V_s ratio (Fig. 8b,c). Hydrocarbon zones are characterized by red color, sand was in yellow color, and shale identified with green color. Comparison of 8a, 8b & 8d, PI attribute was clearly distinctive & having very low values than conventional attribute (Z_p). Hence, the proposed framework successfully revealed HC, sand, and shale using the PI inversion and non-parametric statistical technique.

Numerical analysis. The superiority of the present methodology has been analyzed by comparing the results of non-parametric statistical classification from the different seismic inputs such as Z_p and PI volume generated from the traditional method, which involved an inverse slope of the cross plot of Z_p and Z_s in regression analysis to estimate rotation factor “c”. We have compared these results through the confusion matrix and kappa coefficient. The conventional interpretation results of the non-parametric statistical classification using the Z_p in this study area were taken from⁴⁸. We evaluated the impact of these inputs on the results by comparing each prediction log with the true litho log. Figure 9a,b show the confusion matrix and kappa coefficient of these methodologies. The kappa coefficient determines the match between the prediction values and true values.

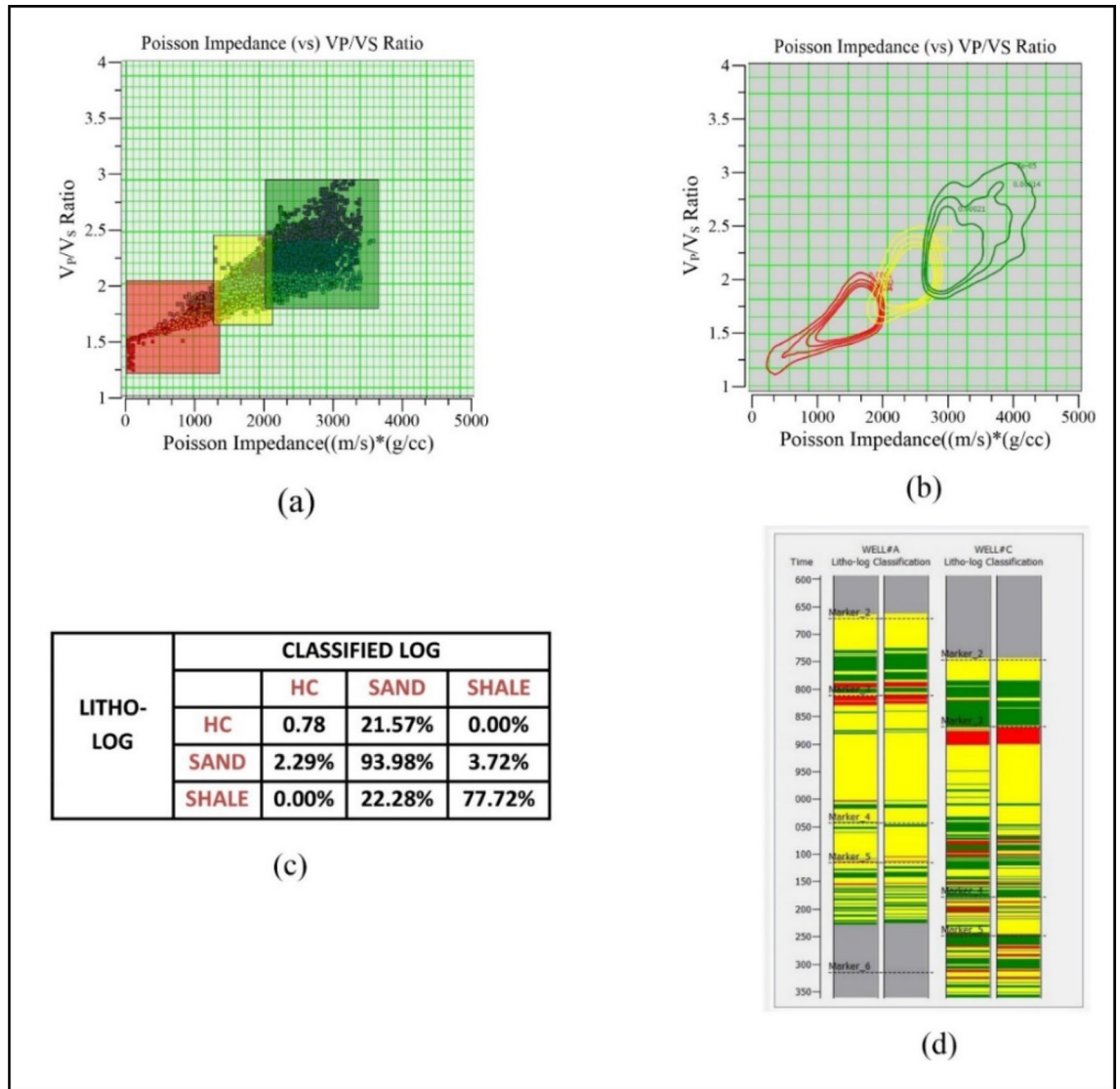


Figure 6. Lithofacies classification procedure and quality measures: (a) cross-plot analysis between PI and V_p/V_s ratio; (b) non-parametric PDFs; (c) confusion matrix; (d) visual inspection of predicted lithofacies at wells (Well#A and Well#C).

Lithofacies class	Poisson impedance (PI) ((m/s) (g/cc))	V_p/V_s ratio
HC	500–1450	1.15–1.82
SAND	1430–2100	1.60–2.45
SHALE	2050–3200	1.78–3.1

Table 2. Lithofacies characterized values of Poisson impedance (PI) and V_p/V_s ratio.

Kappa coefficient.

$$\hat{K} = \frac{M \sum_{i=j=1}^r n_{ij} - \sum_{i=j=1}^r n_i * n_j}{M^2 - \sum_{i=j=1}^r n_i * n_j}$$

where r = number of rows in the confusion matrix, n_{ij} = number of observations in row i , column j , n_i = total number of observations in row i , n_j = total number of observations in row j , M = total number of observations in the matrix.

As observed 9a & b, overall accuracy is higher than the present methodology. It shows the overall accuracy is 83.38%, but the conventional methodology's overall accuracy was only 63.83, as shown in Fig. 9b. The adopted methodology predicted lithofacies better than the conventional methodology in complex fluvial-deltaic deposits

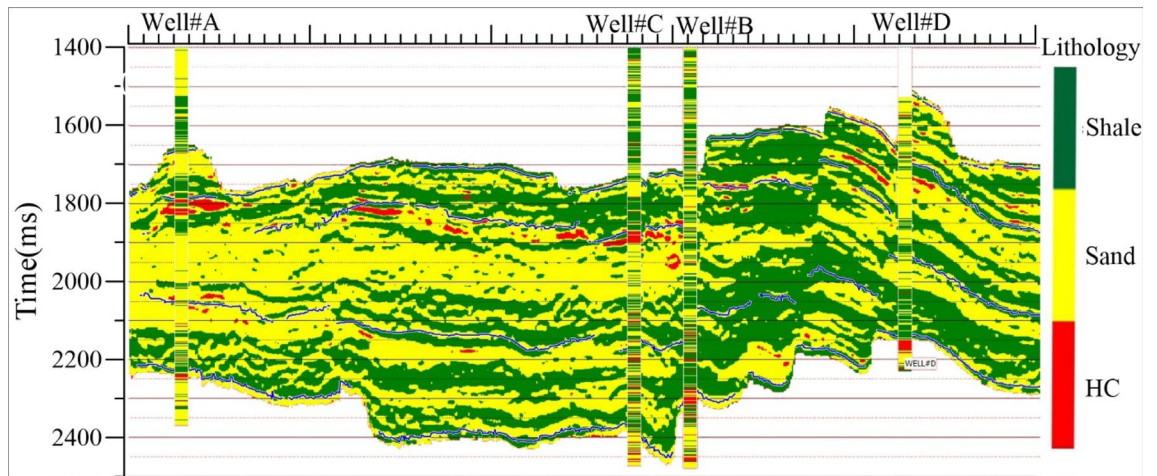


Figure 7. Arbitrary line of lithofacies model intersects at wellbore locations with inserting the true litho-logs.

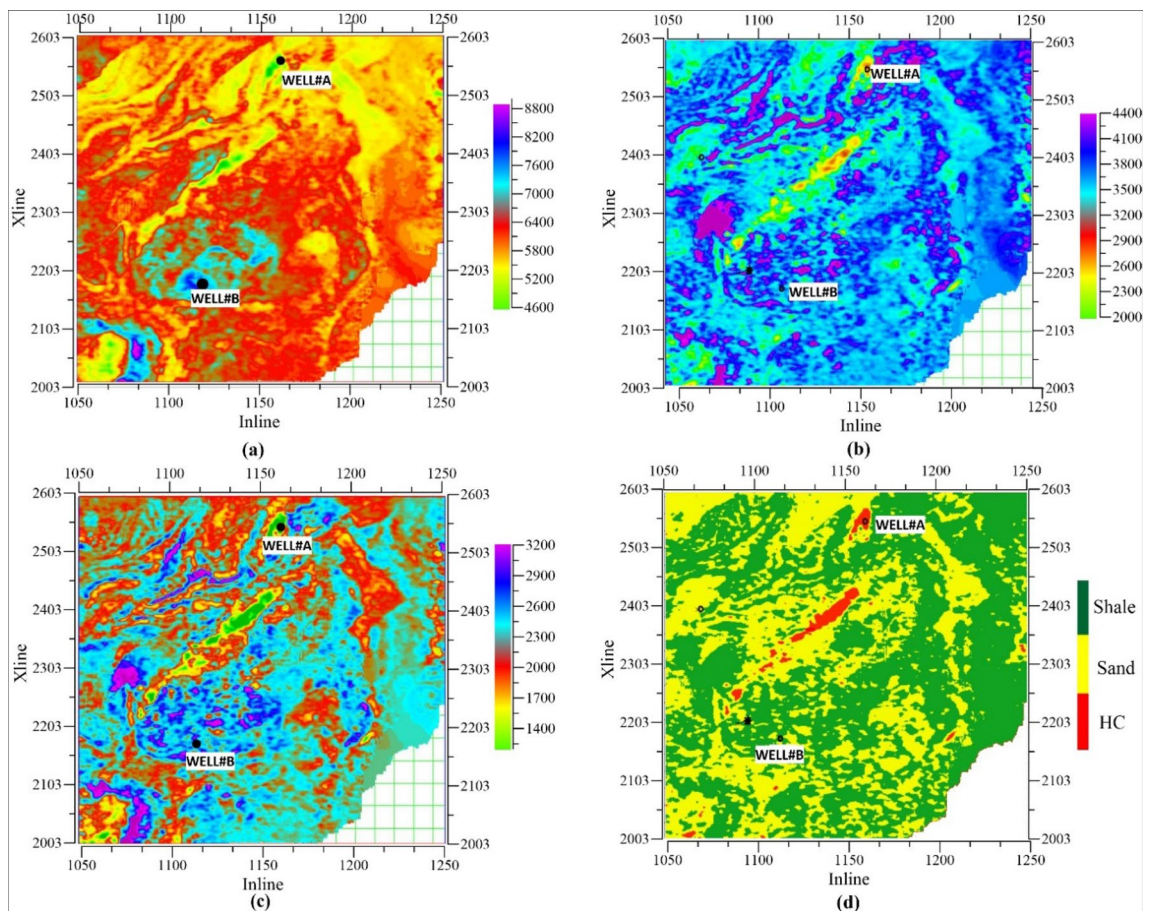


Figure 8. Horizontal slice of seismic attributes (a) acoustic impedance (b) shear impedance (c) Poisson impedance (d) Lithofacies at 1820 ms.

from the Kappa coefficient score. Conventional attributes may be ineffective in distinguishing fluid-saturated zones from non-fluid-saturated zones for complex deposits.

Conclusion

We applied an integrated framework to delineate the lithofacies of complex fluvial-deltaic sandstone reservoirs in an oilfield in Northeast India. Our outcomes proved that the adopted methodology improved the lithofacies distribution in the Upper Assam Basin. Additionally, our findings proved that PI was more effective in estimating hydrocarbon zone than conventional attributes. Seismic elastic attributes are estimated from prestack seismic

(a) Classified Log					
Litho log	HC	SAND	SHALE	Row Total	Litho-log's Accuracy
HC	5263	2895	1842	10000	52.63%
SAND	138	8260	1602	10000	82.60%
SHALE	144	4231	5625	10000	56.25%
Column Total	5545	15386	9069	30000	
Classified log's Accuracy	94.91%	53.68%	62.02%		
Overall Accuracy = 63.83%, Kappa Coefficient = 0.457					

(b) Classified Log					
Litho log	HC	SAND	SHALE	Row Total	Litho-log's Accuracy
HC	7843	2157	0	10000	78.43%
SAND	229	9398	372	9999	93.99%
SHALE	0	2228	7772	10000	77.72%
Column Total	8072	13783	8144	29999	
Classified log's Accuracy	97.16%	68.18%	95.43%		
Overall Accuracy = 83.38%, Kappa Coefficient = 0.751					

Figure 9. Confusion matrix Kappa coefficient and overall accuracy (a) conventional methodology (b) present methodology.

data using the SPSP algorithm. An intermediate procedure of this methodology estimated the rotation factor “c” from the Target correlation coefficient analysis (TCCA) of well-logs. The PI volume and curve were estimated using the rotation factor “c”. Furthermore, the non-parametric statistical technique was applied to estimate PDFs for HC, sand, and shale. Finally, the lithofacies distribution was generated using PDFs, PI volume, and V_p/V_s ratio in Bayesian classification. Our findings correspond to three lithofacies are characterized as HC with PI values (500–1450) ((m/s) *(g/cc) & low V_p/V_s ratio values (1.15–1.82), sand deposits identified with PI values ranging from 1430 (m/s) *(g/cc) to 2100 (m/s) *(g/cc) & V_p/V_s ratio ranging from 1.60–2.45. The shale was characterized modeled with values of PI 2050–3200 (m/s) *(g/cc) & V_p/V_s ratio 1.78–3.1. The results efficiency was verified with numerical analysis through kappa coefficient analysis between conventional results and proposed framework results. This analysis has proven that the adopted methodology provided better lithofacies characterization (Annexure I).

Materials and methodology

The methodology involves simultaneous prestack inversion, Poisson impedance analysis, and non-parametric statistical classification for explicitly identifying the hydrocarbon zone. The seismic prestack inversion technique was applied to predict the seismic elastic properties. Later, Poisson impedance analysis and target correlation coefficient analysis are applied to estimate the Poisson impedance from seismic and well log data. After that, cross plot analysis was conducted to identify different lithologies using the Poisson impedance and VP/VS curves. Finally, non-parametric statistical classification was used to estimate the probability density function. The Bayesian classification method is applied to the model distribution of hydrocarbon zones using Poisson impedance volume.

Simultaneous prestack inversion (SPSI). Seismic subsurface elastic properties such as Z_p , Z_s , ρ , and V_p/V_s ratio are estimated from prestack seismic angle gathers using the simultaneous prestack seismic inversion technique⁴⁹. Conventionally, the outcomes of prestack inversion can be used to optimize, identify prospects, and identify ‘sweet spots’ in field development studies. The prestack inversion procedure began by conditioning the

seismic offset gathers to improve the signal-to-noise ratio by creating the super gather. This strategy reduces random noise while preserving the amplitude versus offset relationships. Using the seismic velocity field, this super gather in the offset domain was transformed to angle-gather for the angles between 0°–45°.

After preparation of angle gather, the well-seismic tie was performed to estimate time to depth relation for depth stratigraphic markers of well log data and time stratigraphic markers of seismic data using the angle-dependent wavelet. Two wavelet extraction methods, such as statistical and well-based, were used to estimate wavelets. First, the statistical method based on the autocorrelation concept was applied to estimate angle-dependent wavelets. These statistical wavelets were convolved with reflectivity from well-log data for synthetic seismic data. This synthetic seismic data is correlated with actual seismic data with a good correlation coefficient at all well locations. Following the acceptable correlation, well-based wavelets are estimated by designing a time-domain operator that is convolved with the actual seismic data. Prestack seismic inversion technique is a process to convert the seismic reflection data into a quantitative depiction of reservoir properties⁵⁰. Simultaneous prestack inversion was explained to estimate the seismic elastic properties⁵¹. Study⁵² performed prestack inversion from the modified reflectivity equation⁵³.

$$RPP(\theta) = A R_p + B R_s + C R_d \quad (1)$$

where $R_{pp}(\theta)$ is reflectivity, $A = (1 + \tan^2 \theta)$; $B = -8(V_p/V_s)^2 \sin^2 \theta$; $C = -0.5 \tan^2 \theta + 2(V_p/V_s)^2 \sin^2 \theta$, $R_p = P$ Reflectivity $= \frac{1}{2} \left[\frac{\Delta VP}{VP} + \frac{\Delta \rho}{\rho} \right] = \frac{\Delta ZP}{2ZP}$, $R_s = S$ - Reflectivity $= \frac{1}{2} \left[\frac{\Delta Vs}{Vs} + \frac{\Delta \rho}{\rho} \right] = \frac{\Delta Zs}{2Zs}$, $R_d =$ density Reflectivity $= \frac{\Delta \rho}{\rho}$.

Poisson impedance (PI) analysis. Poisson impedance analysis was proposed by²⁵, which involved rotating the cross plot of P-impedance (Z_p) and S-impedance (Z_s) for classifying the hydrocarbon zone accurately from other lithofacies. This new parameter called Poisson impedance help as a rock physical parameter in the lithofacies classification. According to⁵⁴, Poisson impedance is similar to the Fluid factor attribute. One particular rotation of the axis of the AI-SI cross-plot precisely distinguishes different lithologies and fluid zones. The PI attribute can estimate using a rotation that links the Poisson's ratio (σ) and density (ρ). The density (ρ) and Poisson's ratio are significant parameters in the reservoir characterization for their low values for hydrocarbon saturated zones. The mathematical notation of the PI attribute is shown in the following equation as explaining a rotation of the AI-SI cross plot to discretize the lithologies.

$$PI = AI - c SI \quad (2)$$

where "c" is a rotation parameter, AI is P-Impedance (Z_p)/Acoustic impedance, SI is Shear impedance (Z_s).

The rotation factor "c" is critical in computing Poisson impedance (PI). The rotation parameter "c" is generally determined using a regression analysis of the AI and SI cross plot for the wet trend¹⁸. However, it will not always provide accurate value due to fitting issues in regression analysis and is also highly influenced by log quality. Another approach, Target correlation coefficient analysis (TCCA), was another approach to obtaining accurate rotation factor "c". The mathematical notation of the TCCA is explained by²⁸. Generally, different logging curves such as Gamma-ray, water saturation, porosity, resistivity, etc., are used to estimate the rotation factor. In this study, the GR log calculated the "c" factor to estimate the Poisson impedance⁵⁵. As introduced²⁹, the correlation coefficients between PI curve with different c-values and GR log.

Non-parametric statistical classification technique & Bayesian modeling. The parametric and non-parametric statistical methods are essential for estimating probability densities. The first requires many assumptions with known PDFs with predefined parameters such as mean value (μ) and deviation (s). The non-parametric statistical classification does not require predefined restrictions as conventional parametric statistical classification. Another advantage is that it uses the data directly without estimating theoretical parameter distribution³⁷. So there is no error and mismatch between the estimated and actual trend of lithology distribution.

This study used non-parametric statistical classification to estimate probabilistic density functions on the lithofacies cross plot between Poisson impedance and V_p/V_s ratio. It was used to avoid the assumptions that are required in the parametric approach. The kernel estimator of the non-parametric classification method was applied to estimate the smoother PDFs from the cross-plot space of Poisson impedance and V_p/V_s ratio⁵⁶. The basic notation to analyze univariate data points is the probability density function for non-parametric data distribution⁵⁷. The density function equation for a random variable that included the probability density function $f(x)$ is as follows

$$P(a < X < b) = \int_a^b f(x) dx$$

For any constants a and b.

By using this density function definition, the probability density function can be constructed. There are two probability density estimators: histogram and smooth density estimator. The kernel density estimation is a simple expanded histogram method. However, the histogram method is discrete and does not provide smooth density functions. In the smooth density estimator, summing all kernel functions in the data provides a smooth representation of the PDFs. The probability density function can be estimated using a non-parametric kernel estimator defined as the following equation for n variable data points (X_1, X_2, \dots, X_n) in the cross plot⁵⁸.

$$f_n(x) = \frac{1}{nh} \sum_{i=1}^n (K) \left(\frac{x - X_i}{h} \right) \quad (3)$$

where K is a kernel function, h is smoother operator length, and sample size indicates by n (X_1, X_2, \dots, X_n).

The smoothing parameter, or bandwidth, h , determines the degree to which the data are smoothed. Minimizing the mean square error yields the optimal bandwidth value⁵⁷. The critical objective is to select an appropriate operator bandwidth (h). Kernel functions that employ Gaussian functions are quite frequent⁵⁹. The Epanechnikov kernel was utilized in this investigation because it had an advantage over Gaussian functions in that it was zero outside of its range. So it has a finite length and is optimal for the minimum variance. Numerous studies discussed that there is no objective technique for determining the optimum bandwidth (h). However, there is a challenge in estimating accurate density function from non-parametric statistical classification, especially in high dimensional spaces. However, the target in this classification is to design and evaluate its performance other than an accurate estimation. Obtaining an accurate density estimate non-parametrically is extremely difficult, especially in high-dimensional spaces. The optimal bandwidth kernel is chosen based on several quality parameters and then created PDFs for different lithologies.

After preparing PDFs, the Bayesian technique converted the seismic attributes (PI and V_p/V_s) into a lithofacies volume by incorporating non-parametric PDFs with seismic PI & V_p/V_s ratio volume⁶⁰. One classification strategy dealing with complex problems is the Bayesian classification method³⁸. It will provide critical knowledge to seismic data classification. The Bayes' rule is essential for statistical data categorization expertise⁶¹. The Bayes' rule is named a unique reservoir characterization tool due to its combined known classification and prediction classification⁶².

Using Bayes' theorem, prior knowledge is included in probability estimates⁶³. This theorem posits that an event's probability is related to estimating lithofacies and prior probability⁶⁴.

For K number of classes, the Bayes' rule for a class " L " is written,

$$p(L|S) = \frac{p(S|L)p(L)}{p(S)} \quad (4)$$

where $p(S) = \sum_{i=1}^k p(S|L)p(L)$.

Where:

- L is a lithofacies type, i.e., shale or sand
- S is a seismic attribute (a combined attribute of Z_p and V_p/V_s ratio)
- $p(L)$ is the a priori probability for class L .
- $p(S|L)$ represents the conditional probability of attributes X knowing we are in class c (for example, distribution of ($Z_p, V_p/V_s$ ratio) in sand), using the notation for conditional probabilities: "|" means "if."
- $p(S)$ is the attributes(S) probability.
- In the prediction of lithology, $p(L)$ is given by the user, and $p(S|L)$ was computed from the PDFs.

Data availability

All data generated or analyzed during this study are included in this article.

Received: 10 March 2022; Accepted: 27 September 2022

Published online: 08 October 2022

References

1. Avseth, P., Mukerji, T. & Mavko, G. *Quantitative Seismic Interpretation*. (Cambridge University Press, 2005). <https://doi.org/10.1017/CBO9780511600074>
2. Radwan, A. E. Modeling the depositional environment of the sandstone Reservoir in the Middle Miocene Sidri Member, Badri Field, Gulf of Suez Basin, Egypt: integration of Gamma-Ray Log patterns and petrographic characteristics of lithology. *Nat. Resour. Res.* **30**, 431–449 (2021).
3. Ismail, A., Ewida, H. F., Al-Ibiary, M. G., Gammaldi, S. & Zollo, A. Identification of gas zones and chimneys using seismic attributes analysis at the Scarab field, offshore, Nile Delta, Egypt. *Pet. Res.* **5**, 59–69 (2020).
4. Arnold, D., Demyanov, V., Rojas, T. & Christie, M. Uncertainty quantification in reservoir prediction: Part 1—Model realism in history matching using geological prior definitions. *Math. Geosci.* **51**, 209–240 (2019).
5. Nagendra Babu, M., Baskey, B., Thota, V. G. & Singh, S. Evaluation of 3D seismic survey design parameters through ray-trace modeling and seismic illumination studies: a case study. *J. Pet. Explor. Prod. Technol.* <https://doi.org/10.1007/s13202-022-01461-w> (2022).
6. Lin, J., Li, H., Liu, N., Gao, J. & Li, Z. automatic lithology identification by applying LSTM to logging data: A case study in X tight rock reservoirs. *IEEE Geosci. Remote Sens. Lett.* **18**, 1361–1365 (2021).
7. Chi, X. & Han, D. Lithology and fluid differentiation using a rock physics template. *Lead. Edge* **28**, 60–65 (2009).
8. Torres, A. & Reverón, J. Integration of rock physics, seismic inversion, and support vector machines for reservoir characterization in the Orinoco Oil Belt, Venezuela. *Lead. Edge* **33**, 774–782 (2014).
9. Ahmed, N., Khalid, P., Ghazi, S. & Anwar, A. W. AVO forward modeling and attributes analysis for fluid's identification: A case study. *Acta Geod. Geophys.* **50**, 377–390 (2015).
10. Liu, N. *et al.* Quantum-enhanced deep learning-based lithology interpretation from well logs. *IEEE Trans. Geosci. Remote Sens.* **60**, 1–13 (2022).
11. Boateng, C. D., Fu, L.-Y. & Danuor, S. K. Characterization of complex fluvio-deltaic deposits in Northeast China using multi-modal machine learning fusion. *Sci. Rep.* **10**, 13357 (2020).

12. Olorunniwo, I., Olotu, S. J., Alao, O. A. & Adepelumi, A. A. Hydrocarbon reservoir characterization and discrimination using well-logs over "AIB-EX" Oil Field, Niger Delta. *Heliyon* **5**, e01742 (2019).
13. Hermana, M., Ghosh, D. P. & Sum, C. W. Discriminating lithology and pore fill in hydrocarbon prediction from seismic elastic inversion using absorption attributes. *Lead. Edge* **36**, 902–909 (2017).
14. Nagendra Babu, M., Ambati, V. & Nair, R. R. An integrated approach to lithofacies characterization of a sandstone reservoir using the Single Normal Simulation equation: A case study. *J. Pet. Sci. Eng.* **208**, 109626 (2022).
15. Maurya, S. P., Singh, N. P. & Singh, K. H. *Seismic Inversion Methods: A Practical Approach*. (Springer International Publishing, 2020). <https://doi.org/10.1007/978-3-030-45662-7>
16. Feng, R., Balling, N. & Grana, D. Lithofacies classification of a geothermal reservoir in Denmark and its facies-dependent porosity estimation from seismic inversion. *Geothermics* **87**, 101854 (2020).
17. Lis-Sledziona, A. Petrophysical rock typing and permeability prediction in tight sandstone reservoir. *Acta Geophys.* **67**, 1895–1911 (2019).
18. Akpan, A. S., Okeke, F. N., Obiora, D. N. & George, N. J. Modelling and mapping hydrocarbon saturated sand reservoir using Poisson's impedance (PI) inversion: a case study of Bonna field, Niger Delta swamp depobelt, Nigeria. *J. Pet. Explor. Prod. Technol.* <https://doi.org/10.1007/s13202-020-01027-8> (2020).
19. Kumar, A., Harith, Z., Kamaruddin, K., Mohd Ramli, A. & Kolupaev, A. Lithology impedance attribute to identify LRLC zone based on well log (2015). <https://doi.org/10.3997/2214-4609.201412293>
20. Wawrzyniak-Guz, K. Rock physics modelling for determination of effective elastic properties of the lower Paleozoic shale formation, North Poland. *Acta Geophys.* **67**, 1967–1989 (2019).
21. Fajana, A. O., Ayuk, M. A., Enikanselu, P. A. & Oyebamiji, A. R. Seismic interpretation and petrophysical analysis for hydrocarbon resource evaluation of 'Pennay' field, Niger Delta. *J. Pet. Explor. Prod. Technol.* **9**, 1025–1040 (2019).
22. Mukerji, T., Avseth, P., Mavko, G., Takahashi, I. & González, E. F. Statistical rock physics: Combining rock physics, information theory, and geostatistics to reduce uncertainty in seismic reservoir characterization. *Lead. Edge* **20**, 313–319 (2001).
23. Datta Gupta, S., Chatterjee, R. & Farooqui, M. Y. Rock physics template (RPT) analysis of well logs and seismic data for lithology and fluid classification in Cambay Basin. *Int. J. Earth Sci.* **101**, 1407–1426 (2012).
24. Nivlet, P. Uncertainties in seismic facies analysis for reservoir characterisation or monitoring: Causes and consequences. *Oil Gas Sci. Technol. Rev. l'IFP* **62**, 225–235 (2007).
25. Quakenbush, M., Shang, B. & Tuttle, C. Poisson impedance. *Lead. Edge* **25**, 128–138 (2006).
26. Wang, L., Zheng, X., Guo, W., He, W. & Xu, J. Effective method of seismic reservoir characterization using normalized Poisson impedance and $\lambda\rho$ attribute. in *SEG Technical Program Expanded Abstracts 2017* 3047–3051 (Society of Exploration Geophysicists, 2017). <https://doi.org/10.1190/segam2017-17640139.1>
27. Zhou, Z. & Hilterman, F. J. A comparison between methods that discriminate fluid content in unconsolidated sandstone reservoirs. *Geophysics* **75**, B47–B58 (2010).
28. Hutahaean, R. A., Rosid, M. S., Guntoro, J. & Ajie, H. Poisson impedance analysis to identify sweet spot shale gas reservoir in field "X". 040004 (2018). <https://doi.org/10.1063/1.5062748>
29. Tian, L., Zhou, D., Lin, G. & Jiang, L. Reservoir prediction using Poisson impedance in Qinhuangdao, Bohai Sea. in *SEG Technical Program Expanded Abstracts 2010* 2261–2264 (Society of Exploration Geophysicists, 2010). <https://doi.org/10.1190/1.3513300>
30. Rosid, M. S., Prasetyo, B. D., Trivianty, J. & Purba, H. Characterization of hydrocarbon reservoir at field "B", South Sumatera by using poisson impedance inversion. *Malays. J. Fundam. Appl. Sci.* **15**, 472–477 (2019).
31. Kim, S., Lee, J., Kim, B. & Byun, J. Effective workflow of Poisson impedance analysis for identifying oil reservoir with similar resistivity log response to neighboring medias. in *SEG Technical Program Expanded Abstracts 2016* 2851–2855 (Society of Exploration Geophysicists, 2016). <https://doi.org/10.1190/segam2016-13856496.1>
32. Yakowitz, S. J. Nonparametric density estimation, prediction, and regression for Markov sequences. *J. Am. Stat. Assoc.* **80**, 215 (1985).
33. Mwenifumbo, C. J. Kernel density estimation in the analysis and of borehole geophysical data. *Log Anal.* **34**, (1993).
34. Corina, A. N. & Hovda, S. Automatic lithology prediction from well logging using kernel density estimation. *J. Pet. Sci. Eng.* **170**, 664–674 (2018).
35. Silverman, B. W. *Density Estimation for Statistics and Data Analysis*. (Routledge, 2018). <https://doi.org/10.1201/9781315140919>
36. Loftsgaarden, D. O. & Quesenberry, C. P. A nonparametric estimate of a multivariate density function. *Ann. Math. Stat.* **36**, 1049–1051 (1965).
37. Ocampo-Duque, W., Osorio, C., Piamba, C., Schuhmacher, M. & Domingo, J. L. Water quality analysis in rivers with non-parametric probability distributions and fuzzy inference systems: Application to the Cauca River, Colombia. *Environ. Int.* **52**, 17–28 (2013).
38. Han, J., Kamber, M. & Pei, J. *Data Mining*. (Elsevier, 2012). <https://doi.org/10.1016/C2009-0-61819-5>
39. Teixeira, R., Braga, I. & Loures, L. G. Bayesian Characterization of Subsurface Lithofacies and Saturation Fluid. in *Proceedings of Latin American & Caribbean Petroleum Engineering Conference* 1278–1282 (Society of Petroleum Engineers, 2007). <https://doi.org/10.2523/108027-MS>
40. Khin, K., Zaw, K. & Aung, L. T. Geological and tectonic evolution of the Indo-Myanmar Ranges (IMR) in the Myanmar region. *Geol. Soc. Lond. Mem.* **48**, 65–79 (2017).
41. Gaina, C., van Hinsbergen, D. J. J. & Spakman, W. Tectonic interactions between India and Arabia since the Jurassic reconstructed from marine geophysics, ophiolite geology, and seismic tomography. *Tectonics* **34**, 875–906 (2015).
42. Gogoi, T. & Chatterjee, R. Estimation of petrophysical parameters using seismic inversion and neural network modeling in Upper Assam basin, India. *Geosci. Front.* **10**, 1113–1124 (2019).
43. Wandrey, C. J. Sylhet-Kopili/Barail-Tipam composite total petroleum system, Assam Geologic Province, India <https://doi.org/10.3133/b2208D> (2004).
44. Baksi, S. K. Stratigraphy of Barail Series in Southern Part of Shillong Plateau, Assam, India: Geological notes. *Am. Assoc. Pet. Geol. Bull.* **49**, (1965).
45. Omudu, L. & Ebeniro, J. Cross-plotting of rock properties for fluid discrimination using well data in offshore Niger Delta. *Niger. J. Phys.* **17**, (2006).
46. Chopra, S., Alexeev, V. & Xu, Y. 3D AVO crossplotting—An effective visualization technique. *Lead. Edge* **22**, 1078–1089 (2003).
47. Nieto, J., Batlali, B. & Delbecq, F. Seismic lithology prediction: a Montney shale gas case study. *CSEG Rec.* **38**, 34–41 (2013).
48. Nagendra Babu, M., Ambati, V. & Nair, R. R. Lithofacies and fluid prediction of a sandstone reservoir using pre-stack inversion and non-parametric statistical classification: A case study. *J. Earth Syst. Sci.* **131**, 55 (2022).
49. Huuse, M. & Feary, D. A. Seismic inversion for acoustic impedance and porosity of Cenozoic cool-water carbonates on the upper continental slope of the Great Australian Bight. *Mar. Geol.* **215**, 123–134 (2005).
50. Schuster, G. T. *Seismic Inversion*. (Society of Exploration Geophysicists, 2017). <https://doi.org/10.1190/1.9781560803423>
51. Hampson, D. P., Russell, B. H. & Bankhead, B. Simultaneous inversion of pre-stack seismic data. in *SEG Technical Program Expanded Abstracts 2005* 1633–1637 (Society of Exploration Geophysicists, 2005). <https://doi.org/10.1190/1.2148008>
52. Russell, B. H., Hampson, D. P., Hirsche, K. & Peron, J. Joint simultaneous inversion of PP and PS angle gathers. *CSEG Rec.* **17**, 1–14 (2013).

53. Fatti, J. L., Smith, G. C., Vail, P. J., Strauss, P. J. & Levitt, P. R. Detection of gas in sandstone reservoirs using AVO analysis: A 3-D seismic case history using the Geostack technique. *Geophysics* **59**, 1362–1376 (1994).
54. Smith, G. C. & Gidlow, P. M. Weighted stacking for rock property estimation and detection of gas*. *Geophys. Prospect.* **35**, 993–1014 (1987).
55. Kim, S. *et al.* Pore fluid estimation using effective workflow of Poisson impedance analysis. *Explor. Geophys.* **51**, 314–326 (2020).
56. Węglarczyk, S. Kernel density estimation and its application. *ITM Web Conf.* **23**, 00037 (2018).
57. Simonoff, J. S. *Smoothing Methods in Statistics.* (Springer New York, 1996). <https://doi.org/10.1007/978-1-4612-4026-6>
58. Faucher, D., Rasmussen, P. F. & Bobée, B. A distribution function based bandwidth selection method for kernel quantile estimation. *J. Hydrol.* **250**, 1–11 (2001).
59. Altman, N. & Léger, C. Bandwidth selection for kernel distribution function estimation. *J. Stat. Plan. Inference* **46**, 195–214 (1995).
60. Doyen, P. *Seismic Reservoir Characterization: An Earth Modelling Perspective (EET 2).* (EAGE Publications bv, 2007). <https://doi.org/10.3997/9789073781771>
61. Richard O. Duda, Peter E. Hart, D. G. S. *Pattern Classification.* in 654 (The MIT Press, 1998).
62. Pendrel, J. & Schouten, H. Facies—The drivers for modern inversions. *Lead. Edge* **39**, 102–109 (2020).
63. Braga, I. L. S., Loures, L. G. & Teixeira, R. G. Workflow for characterization of subsurface lithofacies and saturation fluid. in *10th International Congress of the Brazilian Geophysical Society & EXPOGEF 2007, Rio de Janeiro, Brazil, 19–23 November 2007* 1278–1282 (Brazilian Geophysical Society, 2007). <https://doi.org/10.1190/sbgf2007-249>
64. Hossain, Z., Volterrani, S. & Diaz, F. Integration of rock physics template to improve Bayes' facies classification. in *SEG Technical Program Expanded Abstracts 2015* 2760–2764 (Society of Exploration Geophysicists, 2015). <https://doi.org/10.1190/segam2015-5900545.1>

Acknowledgements

The authors would like to thank Oil India Ltd for providing the data sets for this study.

Author contributions

M.N.B.: Conceptualization, methodology, investigation, interpretation of results, writing and editing manuscript. V.A.: Data and resources. R.R.N.: Resources, review, methodology, and supervision. All the authors comprehended and designed the workflows and wrote the paper.

Competing interests

The authors declare no competing interests.

Additional information

Supplementary Information The online version contains supplementary material available at <https://doi.org/10.1038/s41598-022-21444-5>.

Correspondence and requests for materials should be addressed to M.N.B.

Reprints and permissions information is available at www.nature.com/reprints.

Publisher's note Springer Nature remains neutral with regard to jurisdictional claims in published maps and institutional affiliations.



Open Access This article is licensed under a Creative Commons Attribution 4.0 International License, which permits use, sharing, adaptation, distribution and reproduction in any medium or format, as long as you give appropriate credit to the original author(s) and the source, provide a link to the Creative Commons licence, and indicate if changes were made. The images or other third party material in this article are included in the article's Creative Commons licence, unless indicated otherwise in a credit line to the material. If material is not included in the article's Creative Commons licence and your intended use is not permitted by statutory regulation or exceeds the permitted use, you will need to obtain permission directly from the copyright holder. To view a copy of this licence, visit <http://creativecommons.org/licenses/by/4.0/>.

© The Author(s) 2022